Supplementary Information

Nanosize Effects of Sulfonated Carbon Nanofiber Fabrics for High Capacity Ion-Exchanger

Shinji Imaizumi, Hidetoshi Matsumoto, Minoru Ashizawa, Mie Minagawa, and Akihiko Tanioka**

Department of Organic and Polymeric Materials, Tokyo Institute of Technology, Mail Box S8-27,

2-12-1 Ookayma, Meguro-ku, Tokyo 152-8552

*Corresponding Authors:

HM- Phone +81-3-5734-3640; Fax: +81-3-5734-3640; E-mail: matsumoto.h.ac@m.titech.ac.jp

AT- Phone +81-3-5734-2426; Fax: +81-3-5734-2876; E-mail: tanioka.a.aa@m.titech.ac.jp

Preparation of carbon nanofiber fabrics.

For electrospinning, the fiber diameter depends on the solution properties (e.g., viscosity, conductivity, surface tension, permittivity, and boiling point) and/or operating conditions (e.g., applied voltage, nozzle-to-target distance, and flow rate). In particular, the viscosity and electrical conductivity of the spinning solutions are crucial factors for controlling the fiber diameter. In the present study, we prepared the phenolic resin nanofibers with various diameters through electrospinning by controlling both the viscosity and conductivity of the spinning solution. The composition and properties of the spinning solutions are summarized in Table S1. Fig. S1 and S2 show the effects of the solution viscosity and solution conductivity on the fiber diameter of the carbon nanofibers.

Table S1. The composition and physical properties of the spinning solutions.

Solution	PhR [wt.%]	PVB [wt.%]	Na_2CO_3 [wt.%]	MeOH [wt.%]	Py [wt.%]	Viscosity [mPa sec]	Conductivity [mS m^{-1}]	Fiber diameter [nm]	
								CNF	S-CNF
C1	33.25	1.75	-	59	6	35.8	1.25	1440 ± 400	1450 ± 250
C2	22.50	2.47	0.03	45	30	23.9	4.36	340 ± 100	350 ± 140
C3	17.00	2.98	0.02	48	32	17.7	7.04	230 ± 70	250 ± 90
C4	12.00	2.85	0.15	51	34	11.1	41.50	120 ± 20	140 ± 40
C5	7.50	2.40	0.10	54	36	5.6	46.30	80 ± 20	80 ± 20

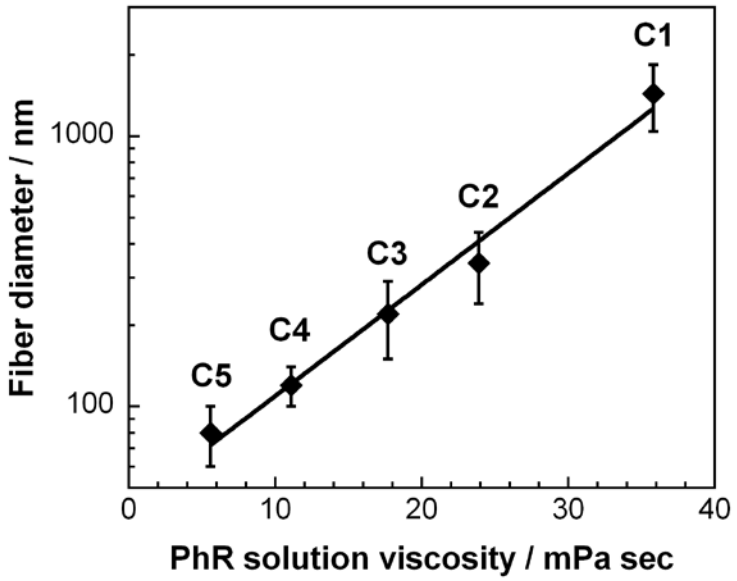

Fig. S1 The effect of the solution viscosity on the fiber diameters of the carbon nanofibers.

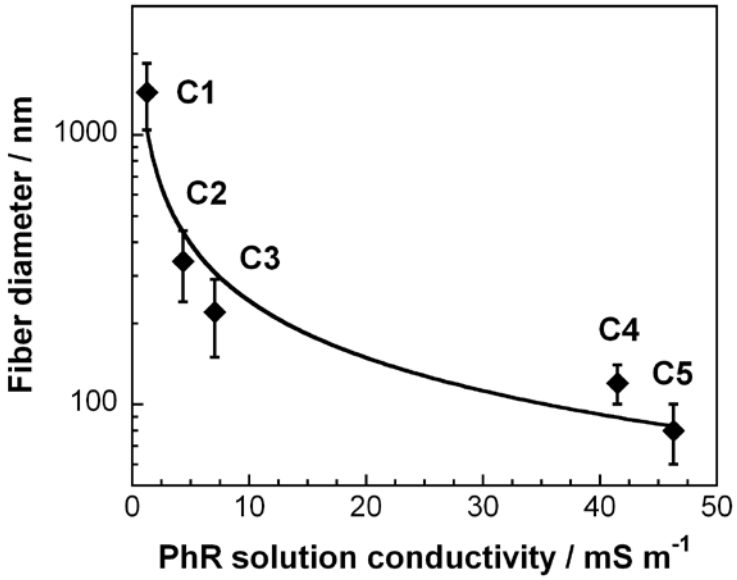

Fig. S2 The effect of the solution conductivity on the fiber diameter of the carbon nanofibers.

X-ray photoelectron spectroscopy (XPS).

We carried out XPS measurements. The S-CNF shows the S_{2p} peak at 168 eV which is attributed to the SO_3H groups (Fig.S3).

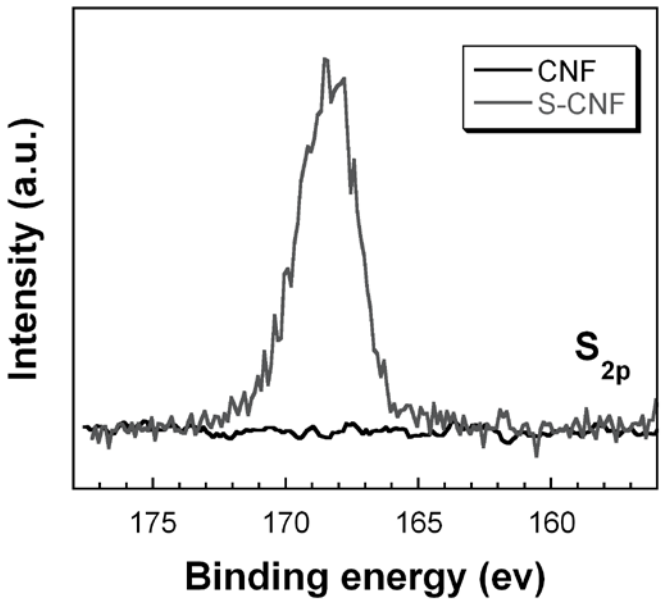

Fig. S3 The XPS S_{2p} spectra of the CNF (D = 1440 nm) and S-CNF (D = 1450 nm).

Pore structure characterization.

The total pore surface areas of the S-CNF fabrics were determined by mercury porosimetry measurements. To predict the effect of the fiber diameter on the total pore surface area of the S-CNF, we used the following equation for a single fiber:

$$S_{TP} = \frac{S_{SA}}{W} = \frac{2\pi\left(D/2\right)^2 + \pi LD}{\pi\left(D/2\right)^2 L\rho} = \frac{2}{\rho}\left(\frac{1}{L} + \frac{2}{D}\right)$$

$$S_{TP} = \lim_{L\to\infty} \frac{2}{\rho}\left(\frac{1}{L} + \frac{2}{D}\right) = \frac{4}{\rho D} \qquad \text{(S1)}$$

where S_{TP} is the total pore surface area of the S-CNF, S_{SA} is the surface area of the S-CNF, W is the weight of the S-CNF, D is the diameter of the S-CNF, L is the length of the S-CNF, and ρ is the density of the S-CNF.

Fig. S4 shows the BET specific surface area for the S-CNF fabrics of various diameters.

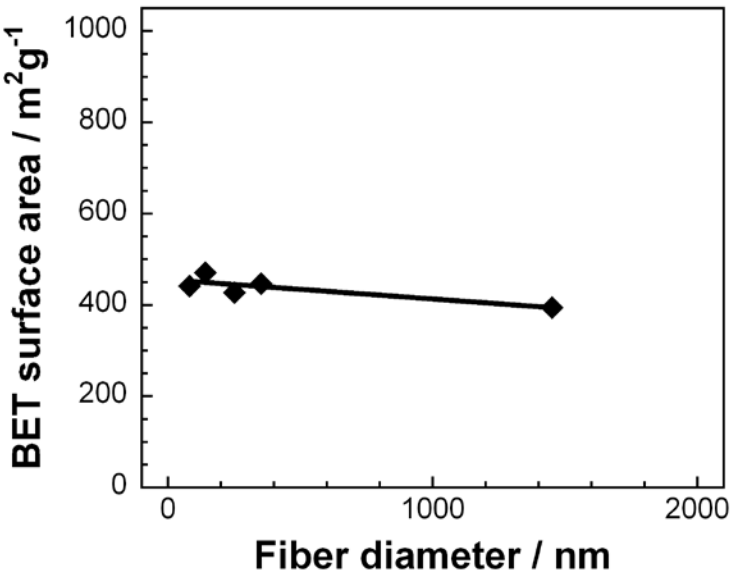

Fig. S4 BET specific surface area for the S-CNF fabrics as a function of the fiber diameter.

Zeta potential measurements.

The zeta potential was obtained from the streaming potential measurements based on the Helmholtz-Smoluchowski equation:

$$\zeta = \frac{dU_{str}}{dp}\frac{\eta\lambda}{\varepsilon_0\varepsilon_r} \qquad \text{(S2)}$$

where U_{str} is the streaming potential, p is the pressure drop across the streaming channel, ε_0 is the vacuum permittivity (8.854×10^{-12} J^{-1} C^2 m^{-1}), ε_r is the dielectric constant of the solution (78.3), η is the solution viscosity (0.8902 mPa sec) and λ is the electrical conductivity of the bulk solution.

The apparent surface charge density of the fabrics was calculated from the ζ–potential using the Gouy-Chapman equation [1]:

$$\sigma_s = \frac{2\varepsilon_0\varepsilon_r kT\kappa}{z_+ e}\sinh\left(\frac{z_+ e\zeta}{2kT}\right) \qquad \text{(S3)}$$

where k is the Boltzmann constant, T is the temperature (= 298K), κ is the reciprocal of the electrical double-layer thickness, z_+ is the valence of the counter-ion, and e is the Coulombic charge. Fig. S5 shows the zeta potential for the S-CNF fabrics of various diameters.

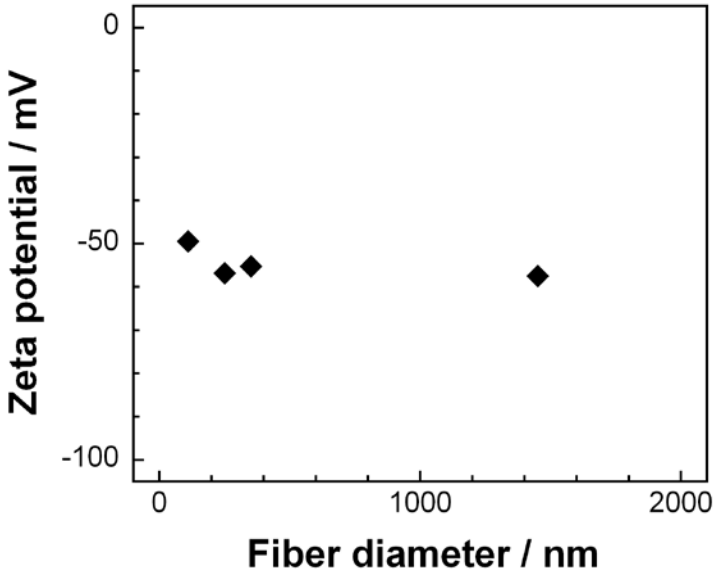

Fig. S5 Zeta potential for the S-CNF fabrics as a function of the fiber diameter (in 1 mM KCl at pH 5.5).

Adsorption experiments.

The S-CNF test fabrics (1 × 1 cm^2) were immersed in 15 ml each of 1, 2, 5, 10, 50, 75, 100, 150, 200, 250, 300 mg/L MB / phosphate equimolal pH standard solutions (pH 6.86) and the adsorption experiments were carried out in a reciprocating shaker for 150 hrs. The dye adsorption was determined by a UV-visible spectroscopy. For comparison, the adsorption experiments for pristine CNFs were carried out. The typical results are shown in Fig. S6. The adsorption capacities of all the pristine CNFs were quite low. This indicates that there are only a few adsorption sites on the pristine CNF.

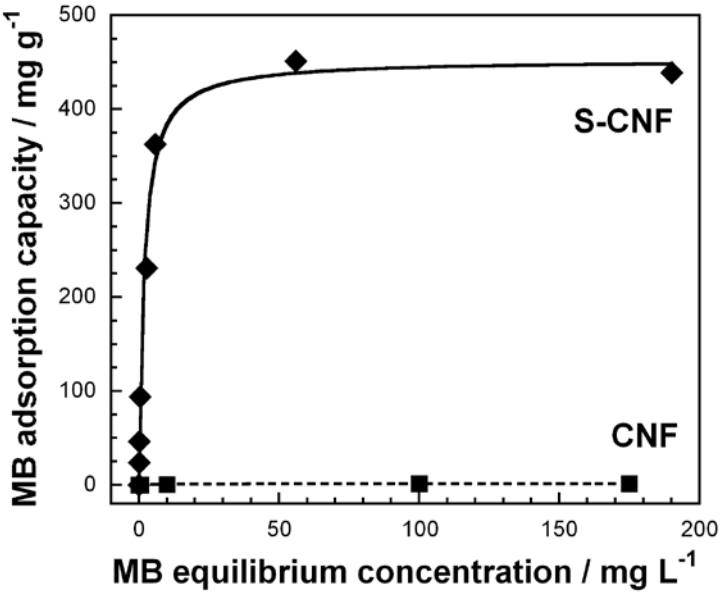

Fig. S6 Adsorption isotherms for MB adsorption over the pristine CNF (D = 1440 nm), and S-CNF (D = 1450 nm).

Fig. S7 shows the Langmuir plots of the isotherms for the S-CNF fabrics of various diameters. The Langmuir plots are used for the determination of q_0 (the maxim adsorption capacity) and b (the affinity coefficient between the sorbent active sites and the adsorbate). The Langmuir plots agreed well with the experimental data (see Fig. 6). For comparison, adsorption experiments for the commercial activated carbon were carried out. These results are shown in Fig. S8.

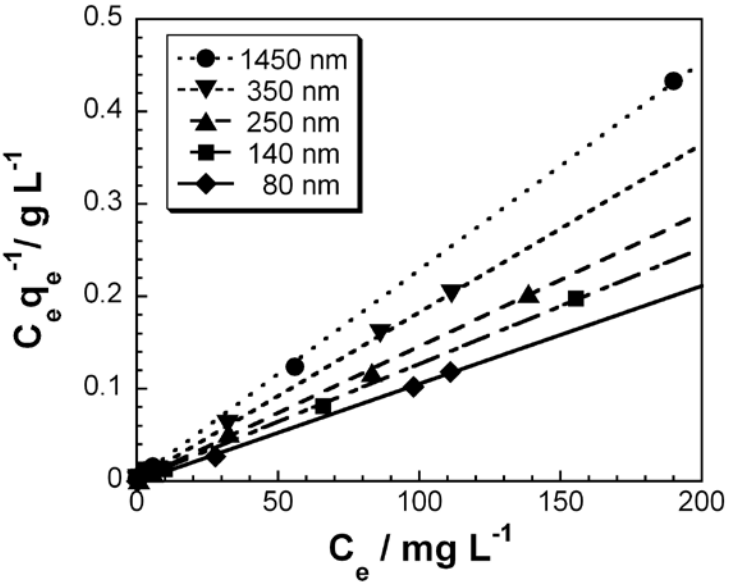

Fig. S7 Langmuir plots of the isotherms for the S-CNF fabrics of various diameters.

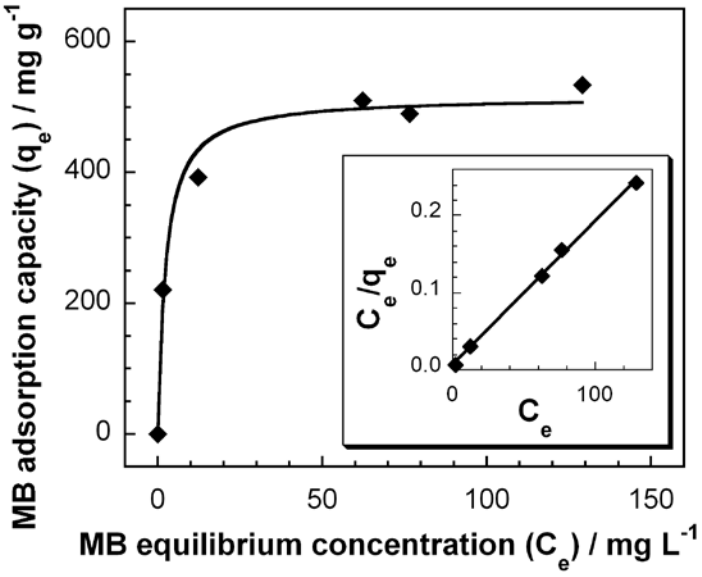

Fig. S8 Adsorption isotherms for MB adsorption over the activated carbon, and (inset) Langmuir plots of the isotherms.

Temperature is also an important factor for the adsorption behavior. Fig. S9 shows the MB adsorption isotherms over the S-CNF fabrics with D = 1450 nm at the temperatures of 30, 45, and 60 ºC. The increasing temperature greatly influences the rate of MB diffusion in the aqueous solution and influences the kinetics of the adsorption behaviors.[2-4] The isotherms in Fig. S9 showed that the MB adsorption capacity of the S-CNFs increased with an increase in the temperature. These results suggested that the adsorption of MB was chemisorption based on the endothermic process which was supported by the following Gibbs free energy ($\Delta G < 0$). [2,5,6]

$$\Delta G = -RT \ln b \qquad \text{(S4)}$$

where R, T, and b are gas constant, temperature, and Langmuir constant (see Table 1), respectively.

In Fig. S10, the thermal stabilities of the S-CNFs and CNFs were examined by thermogravimetric (TG) analysis. From the TG curves for the CNF and S-CNFs, we can find that the both of them showed thermal stabilities below 220 ºC. However, only S-CNFs started weight-loss at 225 ºC. This weight-loss would be due to the decomposition of the SO_3H groups. Typical adsorption processes are carried out less than 200 ºC. Therefore, the thermal stability of the S-CNF is enough for the adsorbents and the carbon-based ion-exchange nanofibers with a good heat resistance are promising materials for highly-efficient adsorption processes and catalysis reactors.

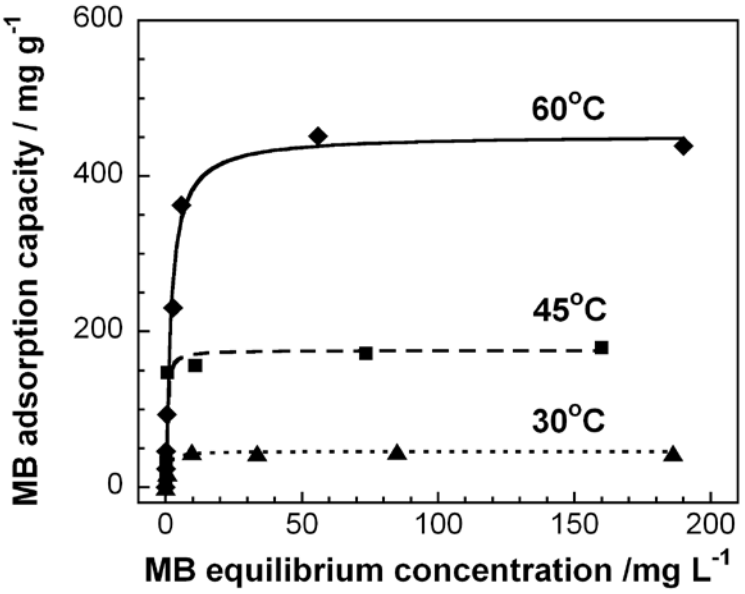

Fig. S9 Effect of temperature on the MB adsorption capacity of the S-CNF fabrics (D = 1.45 μm).

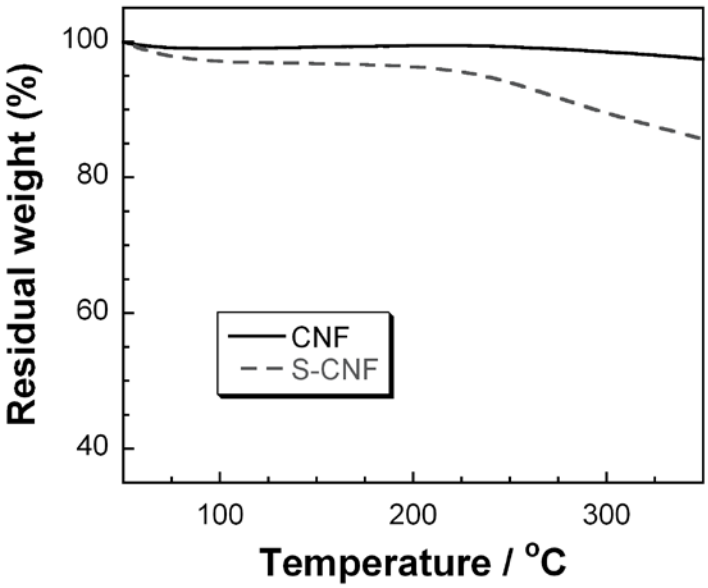

Fig. S10 Thermogravimetric curves for the CNFs (D = 1440 nm) and S-CNFs (D = 1450 nm).

References

[1] H. Matsumoto, Y. Koyama and A. Tanioka, *Langmuir*, 2001, **17**, 3375-3381.

[2] E. Haque, J. W. Jun and S. H. Jhung, *J. Hazard. Mater*., 2011, **185**, 507-511.

[3] A. Rodriguez, G. Ovejero, J. L. Sotelo, M. Mestanza and J. Garcia, *J. Environ. Sci. Health. A*, 2010, **45**, 1642-1653.

[4] X. Han, W. Wang and X. Ma, *Chem. Eng. J*., 2011, **171**, 1-8.

[5] E. Haque, J. E. Lee, I. T. Jang, Y. K. Hwang, J. S. Chang, J. Jegal, S. H. Jhung, *J. Hazard. Mater*., 2010, **181**, 535-542.

[6] S. Wang, L. Li, H. Wu, Z. H. Zhu, *J. Colloid Interface Sci*., 2005, **292**, 336-343.